CORTEX 45 (2009) 340–355

available at www.sciencedirect.com

ScienceDirect

journal homepage: www.elsevier.com/locate/cortex

Special issue: Research report

Coordination of gaze and hand movements for tracking and tracing in 3D

Constantinus C.A.M. Gielen[a,*], Tjeerd M.H. Dijkstra[b], Irene J. Roozen[c] and Joke Welten[a]

[a]Department of Biophysics, Radboud University Nijmegen, Geert Grooteplein 21, EZ Nijmegen, The Netherlands
[b]Institute for Computing and Information Sciences, Radboud University Nijmegen, Toernooiveld 1, ED Nijmegen, The Netherlands
[c]Nijmegen Institute for Cognition and Information, Radboud University Nijmegen, Montessorilaan 3, HR Nijmegen, The Netherlands

ARTICLE INFO

Article history:
Received 29 June 2007
Reviewed 12 November 2007
Revised 14 December 2007
Accepted 25 February 2008
Published online 11 July 2008

Keywords:
Gaze
Two-thirds power law
3D movement
Manual tracking
Smooth pursuit

ABSTRACT

In this study we have investigated movements in three-dimensional space. Since most studies have investigated planar movements (like ellipses, cloverleaf shapes and ''figure eights'') we have compared two generalizations of the two-thirds power law to three dimensions. In particular we have tested whether the two-thirds power law could be best described by tangential velocity and curvature in a plane (compatible with the idea of planar segmentation) or whether tangential velocity and curvature should be calculated in three dimensions. We defined total curvature in three dimensions as the square root of the sum of curvature squared and torsion squared. The results demonstrate that most of the variance is explained by tangential velocity and total curvature. This indicates that all three orthogonal components of movements in 3D are equally important and that movements are truly 3D and do not reflect a concatenation of 2D planar movement segments.

In addition, we have studied the coordination of eye and hand movements in 3D by measuring binocular eye movements while subjects move the finger along a curved path. The results show that the directional component and finger position almost superimpose when subjects track a target moving in 3D. However, the vergence component of gaze leads finger position by about 250 msec. For drawing (tracing) the path of a visible 3D shape, the directional component of gaze leads finger position by about 225 msec, and the vergence component leads finger position by about 400 msec. These results are compatible with the idea that gaze leads hand position during drawing movement to assist prediction and planning of hand position in 3D space.

1. Introduction

A pointing or reaching movement to a target in three-dimensional space constitutes a redundant task at the geometric, kinematic and dynamic level of control. An infinite number of possible hand trajectories can be selected for moving the hand to the target, leading to an infinite set of possible arm postures for every hand location in 3D space.

* *Corresponding author*. Department of Biophysics, Radboud University Nijmegen, Geert Grooteplein 21, 6525 EZ Nijmegen, The Netherlands.
E-mail addresses: s.gielen@science.ru.nl (C.C.A.M. Gielen), t.dijkstra@science.ru.nl (T.M.H. Dijkstra), iroozen@hotmail.com (I.J. Roozen), j.welten@student.science.ru.nl (J. Welten).
0010-9452/$ – see front matter © 2008 Elsevier Srl. All rights reserved.
doi:10.1016/j.cortex.2008.02.009

Although a large number of postures and movement paths are in principle possible, human movements are quite reproducible with a relatively small variability. In order to understand this, postures and movement paths are thought to be the result of some optimization principle. This optimization principle could have a deterministic nature (e.g., minimum jerk (Flash and Hogan, 1985), minimum work (Soechting et al., 1995)) or a stochastic nature (such as minimum variance (Harris and Wolpert, 1998) and the minimum intervention model (Todorov and Jordan, 2002)). Deterministic models can account for the mean properties of movements.

One of the underlying regularities for movements is the two-thirds power law (Viviani and Flash, 1995). This law was first described by Viviani and Terzuolo (1982) for handwriting and drawing movements. It says that the angular velocity $\omega(t)$ of the endpoint is proportional to the radius of curvature $R(t)$ of the end-effector path by the relation $\omega(t) = CR(t)^{2/3}$, where C is a constant. This equation can be rewritten in terms of tangential velocity $v(t)$ and curvature, which results in the relation $v(t) = cR^{1/3}(t)$ (Lacquaniti et al., 1983). Since both equations refer to the same regularity but with different exponents (1/3 instead of 2/3), we will refer to them by using the term ''power law'' instead of two-thirds power law in order to prevent confusion.

The power law has been observed as a phenomenological result in many studies. This has raised the question about its underlying mechanisms. Does it reflect an organizational principle or is it a by-product of other principles that underlie movement generation? Lacquaniti et al. (1983) demonstrated that the power law follows when curved movements are made by a superposition of two orthogonal harmonic oscillators. Later, Wann et al. (1988) suggested that the power law may be a consequence of the smoothness of human movements as maximally smooth (i.e., minimum jerk) movements have speed profiles described by the power law. Triggered by this observation Viviani and Flash (1995) applied the power law and the minimum-jerk model to their data and concluded that the speed–curvature relationship described by the power law is not implied in the minimum-jerk model. This may be related to the fact that the minimum-jerk model was proposed to explain the characteristics of discrete point-to-point movements, whereas the power law was proposed to explain the characteristics of continuous movements. Recently, Flash and Handzel (2007) demonstrated that the natural geometry to describe continuous repetitive movements may not be Euclidean, but equi-affine and that this property predicts piecewise planar movements obeying the power law.

From other research on the power law, the so-called movement segmentation hypothesis arose. Soechting and Terzuolo (1987a, 1987b) provided evidence that 3D rhythmic endpoint trajectories are piecewise planar. Using a curvature criterion as basis for segmentation, they confirmed and extended Morasso's results (Morasso, 1983) that rhythmic movements are segmented into piecewise planar strokes. Similarly, Pelizzer et al. (1992) demonstrated piecewise planarity even in an isometric task. However, recent results by Sternad and Schaal (1999) cast some doubt on the interpretation of planar segmentation. These authors studied drawing movements of elliptical and figure-eight patterns in different orientations in work space. While the endpoint trajectories produced similar segmentation features to those reported in the literature, analysis of the joint angles did not show obvious segmentation but rather continuous oscillatory patterns. In that study they generated movements of a seven-DOF robot by sinusoidal oscillations in the joints, reproducing the same features as observed in human arm movements. Based on these findings, Sternad and Schaal (1999) concluded that segmented patterns do not arise necessarily from a segmented movement generation strategy. In a mathematical analysis they demonstrated that piecewise planar segmentation can be interpreted as an epiphenomenon of oscillatory joint space trajectories and the nonlinear kinematics of the human arm.

The hypothesis of planar segmentation implies that the power law applies to movements in 2D and suggests that 3D movements are made by a concatenation of 2D segments. However, a systematic study of movements with different 3D shapes has not been done yet. Many studies investigated the power law by studying movements that were basically in 2D, such as Soechting and Terzuolo (1987a) and Lacquaniti et al. (1983), who studied planar ''figure eight'' movements, Wann et al. (1988) who studied circle movements on a planar sheet of paper, Sternad and Schaal (1999) and Schaal and Sternad (2001) who studied 2D ellipses in various orientations, Richardson and Flash (2002) who studied ellipses, figure-eight shapes and cloverleaves, and Flash and Handzel (2007), who studied cloverleaves, ''figure eights'' and double ellipses. Little work has been done on movements in three dimensions. Morasso (1983) and Soechting and Terzuolo (1987b) studied scribbles in 3D. In addition, Todorov and Jordan (1998) studied 3D movements, but only small movements (within 10^3 cm^3). In this study we used 3D curved movements to address the question whether the power law applies to 2D movements (in agreement with the planar-segmentation hypothesis) or whether the power law applies to movements in 3D. The latter would be compatible with the ideas proposed by Flash and Handzel (2007) who developed a theory using affine differential geometry that applies to 3D movements and which predicts the power law as an emergent property. Therefore, the first aim of this study was to explore whether the power law applies to 3D movements in different orientations, or whether a restriction to piecewise planar 2D movement segments gives a better description.

In order to test the validity of the power law for movements in 3D we evaluated three variants of the power law. These variants arise from different ways to calculate (tangential) velocity and curvature. The first variant of the power law is a direct generalization of the power law and assumes that movements are planar. This is obvious for movements along a planar ellipse. Movements in 3D like the cone and the elliptical spiral can be conceived of as a superposition of a planar movement (a spiral or an ellipse, respectively) and a velocity in the direction orthogonal to the plane with the spiral and ellipse. In this model the tangent velocity was defined as the tangent velocity to the planar spiral/ellipse. For the Cassini shapes, the tangent velocity was defined as the velocity in the plane of the Cassini shape, i.e., any velocity components orthogonal to the plane were ignored. Curvature was defined as the reciprocal of the radius of a tangent circle.

Since the curvature equals the inverse of the best-fitting planar circle, we call this model *the 2D-planar curvature model*.

The second variant assumes that tangential velocity is the vector length of 3D velocity in the tangent plane of the endpoint trajectory. The curvature in this model is calculated analogous to the *2D-planar curvature model*, i.e., the inverse of the best-fitting planar circle. Since this model incorporates the 3D tangential velocity, we call this second model the *3D-planar curvature model*. The third variant calculates the tangential velocity as the vector length of the 3D tangential velocity of the endpoint trajectory (like the *3D-planar curvature model*), but computes the curvature in a more advanced manner. This takes into account the rate of change of the planar circle, called torsion. This curvature measure is called total or third curvature (Stoker, 1989) and reflects the 3D-curvature of paths. The third variant, which takes into account the 3D tangential velocity and total curvature, is defined as *total curvature model*.

Although the power law has been investigated frequently for arm movements, studies on other motor systems are scarce. de'Sperati and Viviani (1997) reported that smooth pursuit eye movements were most accurate with a small number of saccades when the subject had to track a target that moves in space with a curvature–velocity relationship compatible with the power law. Based on these results these authors suggested that the power law may reflect a general neuronal mechanism that underlies the control of various motor systems such as the eye and arm.

If the power law applies to movements in 3D, as predicted by Flash and Handzel (2007), this implies that the relationship between tangential velocity and curvature is the same for all 3D movement directions. If that same result would equally apply to eye movements, as suggested by de'Sperati and Viviani (1997), this might be in conflict with the fact that the dynamics of eye movements in direction and vergence is very different. Gaze shifts in a natural environment generally require binocular eye movements that have combined directional and depth components. In such responses both the saccadic and vergence subsystems are invoked to ensure that the respective lines of sight of the two eyes ultimately will intersect on the target of interest. It has become evident that, when tested in isolation, these two subsystems exhibit markedly different dynamic characteristics (see for example Collewijn et al., 1997; Erkelens et al., 1989a, 1989b; Yarbus, 1967). Saccades responsible for the control of rapid changes of gaze in direction (version) are fast and conjugate (the eyes move equally in the same direction), whereas vergence responses (which rotate the eyes by equal amounts in opposite directions) required as a result of changing target distance are disconjugate and relatively slow. These differences have led to the suggestion that conjugate and disconjugate eye movements use different neurophysiological substrates (Leigh and Zee, 1983). The hypothesis of separate neural control systems has gained support with the discovery of vergence-related neurons in the midbrain (Mays, 1984). Based on these results, it is not trivial that the trajectories of eye movements are the same for arbitrary directions in 3D space. In order to investigate the nature of eye movements during hand movements in 3D and in order to investigate the coordination between eye movements and hand movements, we have measured binocular eye movements to determine the position of gaze.

In summary, the aims of our study were (1) to compare adherence of three-dimensional finger movements to the power law and to find the best model to describe these movements, and (2) to test the hypothesis that the relationship between finger movements and gaze is the same for all directions in 3D space. This was investigated by instructing subjects to track a target moving in 3D or to move the finger along a curved path in 3D space while measuring gaze and finger position.

2. Methods

Subjects were asked to track a target, moving in 3D, with the tip of the index finger or to move the index finger along a completely visible path in 3D space. The position of the finger tip and that of 3D gaze was measured to compute the tangential velocity and the curvature and to fit these data to three distinctive models to see which of them gave the best fit.

2.1. *Subjects*

Thirteen participants (five females and eight males; age between 20 and 53, average age 28) volunteered and gave their written informed consent prior to inclusion. All subjects were right-handed and none of the subjects had any known neurological or motor disorder. All subjects reported normal binocular vision. Three subjects (authors of this paper) were familiar with the purpose of the experiment. The results of these subjects were not different from those of the other subjects. All experiments were approved by the Medical Ethical Committee of the University Medical Center Nijmegen.

Ten subjects (among them three authors) participated in the first experiment, where only position of the arm (shoulder, elbow, tip index finger) was measured. Five subjects (among them one author) participated in the second experiment, where both gaze position and position of the index finger tip were measured. Two subjects participated in both experiments.

Subjects were seated in a chair with a high rigid and straight backrest. Subjects were strapped to the back of the chair with two belts crossing the trunk from the upper right (left) shoulder to the lower left (right) hip, such that the position of the shoulders and trunk was fixed. These precautions were taken to ensure that subjects were free to make movements in the elbow and shoulder joint, but could not move the shoulders in space. The chair was positioned such that the subject's right shoulder was at a distance of 70 cm from the centre of a projection screen (Fig. 1).

2.2. *Stimuli*

Quasi 3D visual stimuli were generated using a virtual reality system. A 3D shape was programmed in a PC and two images of that shape were produced using red/green stereograms. Two projections of the images in red and green, as viewed from the right and left eye, respectively, were projected on a translucent screen (size 2.5×2 m) with an LCD projector (Philips ProScreen 4750) (see Fig. 1), taking into account the

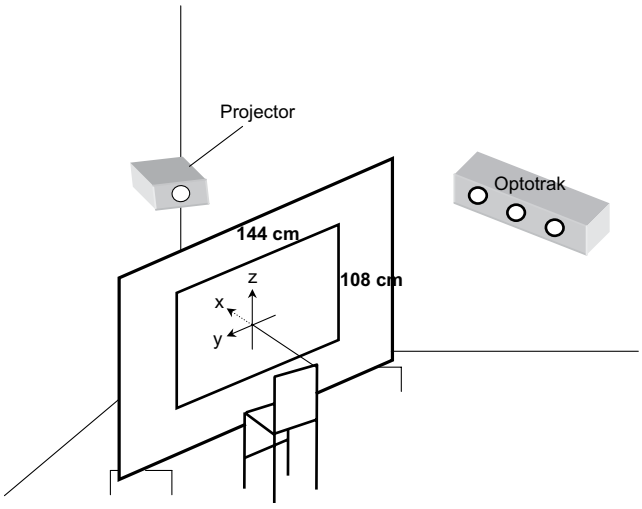

Fig. 1 – Schematic overview of experimental setup with the video-projection system (Philips ProScreen 4750), Optotrak 3020 system and the position of the chair relative to the projector screen. The back of the chair was at a distance of 70 cm from the screen. The head of the subject was adjusted such that it was right in the middle, in front of the projection area. The X-, Y-, Z-coordinate system was located at the right shoulder of the subject. Since drawing this coordinate system at the position of the right shoulder of the subject would interfere with the shape of the chair, the coordinate system is shifted along the X-axis in Fig. 1 for reasons of clarity.

distance between the eyes of the subject. When viewed through red and green '3D-glasses', disparity between the red and green images provides the percept of depth. The size of the computer-generated image on the screen was 144 cm (horizontal) by 108 cm (vertical).

2.3. *Experiment 1*

Subjects were tested in two experiments. In the first experiment, subjects were asked to move the tip of the index finger along a path in 3D. Three different shapes were presented: planar circular spirals, circular conical helices and elliptical cylindrical helices, referred to as spiral, cone and elliptical spiral, respectively. Each shape was presented in three orientations in space with the projection of the circular rotations in the *y*–*z* plane, *x*–*z* plane and *x*–*y* plane, referred to as frontal, sagittal and horizontal plane (see Fig. 2), with the depth dimension for the cones and elliptical spirals in the *x*-, *y*-, and *z*-direction, respectively. Each shape is shown with two or five windings. In all we have three shapes in three orientations, each with two possible winding numbers, resulting in 18 different stimulus shapes.

The paths for the various stimuli were generated by the following equations:

2.3.1. *Planar spiral*

$$X(t) = R\alpha(t)\cos(\omega t)$$

$$Y(t) = R\alpha(t)\sin(\omega t)$$

with $R = .25$ m and with $0 \le t \le 4\pi/\omega$ and $\alpha(t) = (\omega/4\pi)t$ for two windings and with $0 \le t \le 10\pi/\omega$ and $\alpha(t) = (\omega/10\pi)t$ for five windings. With this definition, the spiral lies in the horizontal plane. For presentation in the frontal and sagittal plane, the spiral was rotated along into the *y*–*z* or *x*–*z* plane, respectively.

2.3.2. *Cone*

The cones can be described by a spiral movement in a plane and a constant velocity orthogonal to that plane. They are defined by

$$X(t) = R\alpha(t)\cos(\omega t)$$

$$Y(t) = R\alpha(t)\sin(\omega t)$$

$$Z(t) = .3 - vt$$

with $R = .25$ m and with $0 \le t \le 4\pi/\omega$, $\alpha(t) = (\omega/4\pi)t$ and $v = 0.6\omega/4\pi$ for two windings and $0 \le t \le 10\pi/\omega$, $\alpha(t) = (\omega/10\pi)t$ and $v = 0.6\omega/10\pi$ for five windings.

2.3.3. *Elliptical spiral*

$$X(t) = R_x\cos(\omega t)$$

$$Y(t) = R_y\sin(\omega t)$$

$$Z(t) = .3 - vt$$

with $R_x = .125$ m and $R_y = .25$ m. For the shapes with two windings, the velocity v and angular velocity ω were chosen such that $0 \le t \le 4\pi/\omega$ and $4\pi v/\omega = 0.6$ m. For the shapes with five windings, the relation was $0 \le t \le 10\pi/\omega$ and $10\pi v/\omega = 0.6$ m.

With these definitions the spiral is in the horizontal plane relative to the subject and the cone and elliptical spiral consists of a planar spiral or elliptical path, respectively, with a constant velocity superimposed in vertical direction. Each of these shapes was presented in three orientations, which implies that the *x*-, *y*- and *z*-components were interchanged.

Each of the 18 shapes was presented in random order and the complete shape was visible to the subject. The subject was instructed to move the tip of the right index finger tip along the shape at a comfortable speed. No particular instruction regarding speed was given. When the subject had completed a full movement along the shape, he had to reverse the tracing movement backwards in the reversed direction. For the spirals, the movement had to start in the middle, increasing the radius of the spiral movement. For the cones, the movement had to start at the top. The shapes with two windings were traced 8 times in forward direction and 7 times in backward direction (resulting in a total of 15 movement trajectories for each shape in each orientation). The stimuli with five windings were traced 6 times in both forward and backward direction giving a total of 12 movement trajectories for each shape with five windings in each orientation. Between each set of tracing movements for a particular shape, subjects were allowed to relax for about 2 min to prevent fatigue.

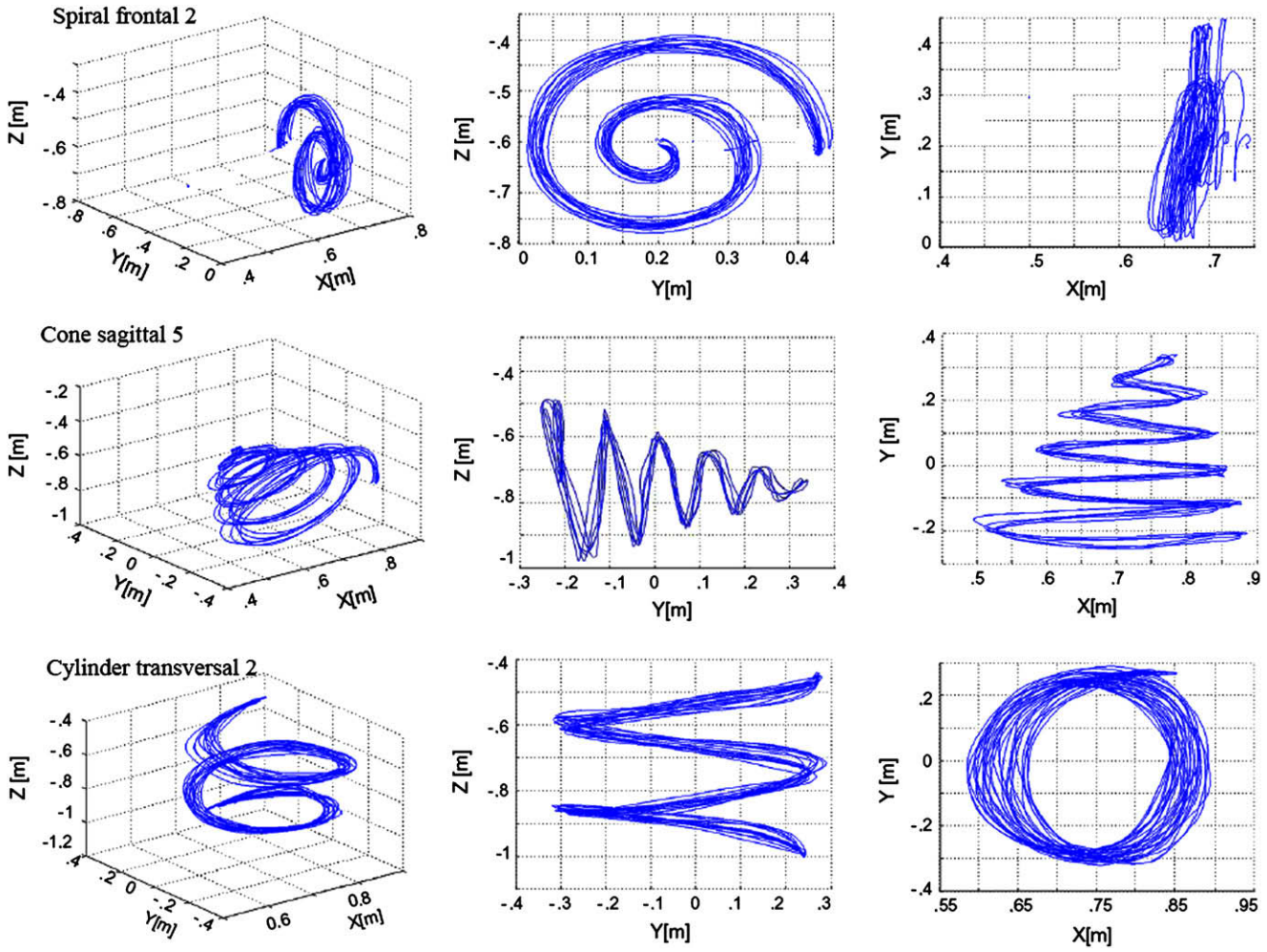

Fig. 2 – Quasi-three-dimensional view (left column) and two-dimensional projection on the z–y plane (front view; middle column) and y–x plane (viewed from the top downward; left column) of three shapes in three orientations. Upper row shows data for the planar spiral in the frontal plane; the middle row shows data for a cone with five windings with a constant velocity in horizontal (Y) direction; bottom row shows data for a cylinder with two windings with a constant velocity in the vertical (Z) direction.

2.4. *Experiment 2*

In the second experiment, both position of the index finger and 3D gaze position were measured. Since the duration of these experiments had to be limited to about 45 min, the number of movements had to be restricted. In these experiments subjects were instructed either to track a small spherical target moving along a Cassini shape, a cone, or an elliptic spiral (tracking condition) or to move the finger along the completely visible Cassini shape, cone or elliptic spiral (tracing condition).

The Cassini shapes (see also Mrotek et al., 2006; Flanders et al., 2006) were composed of planar curved segments. The equations used to make the Cassini shape were

$$X(t) = R(1 + A\cos(2\omega t))\cos(\omega t)$$

$$Y(t) = 1.5R(1 + A\cos(2\omega t))\sin(\omega t)$$

with $A = .5$ cm and $R = 10.0$ cm. The Cassini shapes were presented in the frontal plane and in an oblique orientation, rotated 45° around the horizontal (Y) axis through the centre of the shape, such that the bottom of the shape was closer to the subject than the upper part of the Cassini shape.

The shape of the cones and elliptical spirals were the same as in the first experiment.

2.5. *Measurement system*

Infra-red light-emitting diode markers were placed on the right shoulder, on the elbow and on the tip of the index finger. The 3D position of these three markers was measured with an OPTOTRAK 3020 system (Northern Digital Inc.) at a sample rate of 200 Hz and with an accuracy of .1 mm in all dimensions. Data were collected in the three-dimensional coordinate system of the OPTOTRAK system and saved for offline analysis.

In the analysis, the 3D coordinates of the infra-red light-emitting markers in OPTOTRAK coordinates were transformed into a right-handed coordinate system relative to the

subject with the x-, y-, and z-axis in the same directions as in Fig. 1 but with the origin in the shoulder of the subject. Therefore, the origin of the 3D position coordinate system coincided with the position (−.7, 0, 0) (units in m) of the stimulus coordinate system.

Velocity, acceleration and jerk were obtained from the 3D position data using the Savitzky-Golay filter (sgolay) in MATLAB. The order of this filter was set to $M = 4$, and the frame sizes (L) were 25, 51 and 77 data points to obtain velocity, acceleration and jerk, respectively. With this filter, one effectively fits a polynomial of order M to L data points using a least-square criterion. From the fitted polynomial one can obtain analytical derivatives up to order $M - 1$.

Gaze was measured using the scleral search-coil technique in two eyes simultaneously in a large magnetic field (Remmel Labs.). This system consists of a cubic frame of welded aluminum of $3 \times 3 \times 3\ m^3$, which produced three orthogonal magnetic fields at frequencies of 48, 60 and 80 kHz. During the experiments subjects were placed such that the search coils were close to the centre of the large magnetic field, where the magnetic fields are homogeneous. No instruction was given to the subjects regarding their eye movements during tracking or tracing of the 3D shapes.

The calibration of the coils was done in two steps: the first step (''the calibration trial'') was used for to fit the parameters for each coil (eye) separately to convert the signals from the amplifiers into degrees for azimuth and elevation. The calibration trial consists of 25 targets: the targets were arranged at three circles with radius 8.05, 16.10 and 24.15 cm with eight targets each (every 45°), concentric around a central target in the straight-ahead direction and one target at the common centre of these circles. These targets were projected on the screen, which was at a distance of 70 cm from the shoulders of the subject. The targets were presented subsequently for 3.5 sec. The output signals of the coils were filtered by a fourth order Bessel low-pass filter (3 dB cut-off frequency at 150 Hz). The signals of the coils were sampled at 100 Hz. With this setup, the mean calibration errors for azimuth and elevation for each eye were smaller than .1° over a range of ±45° in both directions.

The second step (''the control trial'') was used to provide an independent measure for the accuracy of the calibration and to determine the accuracy of gaze measurement in 3D. The control trial existed of 24 targets, which were arranged at two circles with a radius 12.5 and 25.0 cm with four targets each (every 90°), concentric around the straight-ahead direction at a depth of −5, −25 and −45 cm relative to the screen (i.e., in a direction toward the subject). The subject was instructed to fixate at each of the targets. Accuracy of the 3D measurement of gaze was defined as the mean error between the actual target position (i.e., the position programmed on the stimulus generation computer) and the gaze position obtained after transformation of the coil signals using the calibration data obtained in the calibration trial.

Gaze position was defined as the intersection of the fixation directions of the two eyes or, if the fixation directions of the two eyes did not intersect, gaze was defined as the position halfway between the nearest two points along the fixation directions of the eyes. This caused relatively large errors for the depth direction of gaze position. Since the intersection point can be measured more accurately for near gaze positions than for far gaze positions, the accuracy of gaze position in depth depends on the distance of gaze position (about 2 mm for fixation at 25 cm from the cyclopean eye to about 5 mm at a distance of 75 cm). On average gaze could be determined with an accuracy of 3 mm in the depth direction and with an accuracy better than 1 mm for azimuth and elevation.

One should realize that the first step of the calibration only focuses on the accuracy of azimuth and elevation for each eye, but not on the accuracy of the depth estimate of gaze. Since noise in the two coils might cause that the two lines of sight do not intersect, we determined fixation as the position halfway between the two nearest neighbours on the two lines of sight. The second step was necessary to obtain an estimate of the accuracy of the procedure to estimate the distance of fixation (depth component of gaze).

2.6. Position, velocity, curvature and torsion

Curvature was calculated using the Frenet equations (Stoker, 1989). If $X(s)$ represents a curved path as a function of the arc length s, the tangent vector $\dot{X}(s) = d/ds(X(s))$ is a unit vector in the direction of the tangent to the path. The second derivative $\ddot{X}(s) = d^2/ds^2(X(s))$, called the normal vector, is orthogonal to $\dot{X}(s)$ and represents the direction of change of the tangent vector $\dot{X}(s)$ along the curved path in s. The higher the curvature of the path, the larger the second derivative $\ddot{X}(s)$. Therefore, the size of $\ddot{X}(s)$ is called the curvature $\kappa = |\ddot{X}(s)|$. The reciprocal of the curvature is the radius of the curved path: $R = 1/\kappa$. The Frenet frame is a local orthogonal coordinate system to a curved path, which is defined by the unit tangent vector $\vec{e}_t$ to the path and the unit normal vector $\vec{e}_n = \ddot{X}(s)/|\ddot{X}(s)|$. The plane, defined by the tangent vector and the normal vector is called the osculating plane. Since the tangent vector points along the forward direction of the curve, the orientation of the osculating plane changes along the curved path. The binormal vector $\vec{e}_b = \vec{e}_t \times \vec{e}_n$ is the third Frenet vector. It is always orthogonal to the tangent and normal vector and therefore, also orthogonal to the osculating plane. The first derivative of the binormal measures the change in orientation of the osculating plane as a function of path length. Therefore, the first derivative of the binormal is a measure for the rate of change of the curve from a curve lying completely in the osculating plane. This deviation is captured by the torsion τ, which is defined by $\tau = |\dot{e}_b| = 1/\kappa^2(|\dot{X}(s) \cdot (\ddot{X}(s) \times \dddot{X}(s))|)$. If differentiation with respect to time t is used, instead of differentiation with respect to arc length s, the expression for torsion becomes: $\tau = X'(t) \bullet (X''(t) \times X'''(t))|X''(t) \times X''(t)|^{-2}$ with $X'(t) = (d/dt)X(t)$, $X'(t) = (d^2/dt^2)X(t)$, etc.

If the torsion is 0, the curved path is a path in a plane (like for the spiral). The curvature κ, torsion τ and tangential velocity v are related to the tangent vector, normal vector and binormal vector by the Frenet equations

$$\begin{aligned} \frac{d}{dt}\vec{e}_t &= +\kappa v \vec{e}_n \\ \frac{d}{dt}\vec{e}_n &= -\kappa v \vec{e}_t + \tau v \vec{e}_b \\ \frac{d}{dt}\vec{e}_b &= -\tau v \vec{e}_n \end{aligned} \quad (1)$$

The tangential velocity v, curvature κ and torsion τ describe how the Frenet frame turns and twists as it moves along the space curve. By construction, the Frenet frame does not depend on the specific choice of the Cartesian coordinate system and the result that curvature and torsion describe the intrinsic geometric properties follows directly. The curvature and torsion (as functions of arc length) jointly constitute a complete 3D description of space curves, up to Euclidean isometries.

The curvature κ is defined by the normal vector $\ddot{X}(s)$ to the tangent and represents the curvature to a movement path in a local, two-dimensional plane (the osculating plane). Therefore, the curvature κ is a two-dimensional measure for curvature. The torsion τ measures the rate at which the osculating plane turns about the tangent vector to the curve and can therefore be viewed as the three-dimensional measure for curvature. The torsion by itself is not a good predictor for tangent velocity as many experiments on the power law were done for 2D figures for which the torsion is 0. Thus, we sought a curvature measure that combines curvature κ and torsion τ and used the total curvature defined by $K = \sqrt{\kappa^2 + \tau^2}$. The total curvature includes the planar curvature, but also incorporates deviations out of the plane (like in the cone stimulus), which are captured by torsion. The total curvature is sometimes called the third curvature, the curvature and torsion being the first and second curvature. The total curvature equals the 2D curvature for planar figures and encompasses the torsion.

In closing we give the order of magnitude of our curvature measures for the stimuli that we used. The torsion τ is 0 for the spiral and, therefore, should be close to 0 for tracing movements along the spiral stimuli. The planar curvature κ of the path of the index finger decreases if the finger moves along the spiral starting from the middle. The planar curvature κ is 4 m^{-1} or larger for the planar spiral and the cone. κ varies between 4 and 8 m^{-1} for the elliptical spiral. For the planar spiral, the total curvature K is equal to the planar curvature κ. For the cone and elliptical spiral stimuli, the torsion τ is not 0. The value of torsion τ is between .74 and 21 m^{-1} for the cone with two windings and between .30 and 21 m^{-1} for the cone with five windings, respectively. For the elliptical spirals torsion τ is .60 and .24 m^{-1} for two and five windings, respectively. The curvature κ, and therefore also the total curvature K, changes along the path of the cone and the elliptical spiral.

2.7. Data analysis and model fitting

The data are analyzed in three different ways to test three different models for the relation between tangential velocity and curvature. For all three models a regression has to be calculated between the logarithm of velocity and logarithm of the inverse of curvature. This implies that the regression is sensitive to noise if either velocity or curvature approaches 0. According to the power law, velocity will become small when the curvature is large, and velocity should become infinitely large for movement segments that approximate a straight line (i.e., at inflection points, when curvature crosses 0). For that reason, data were excluded from analysis when the tangential velocity was less than .05 m/sec and when curvature was less than 2 m^{-1} (radius larger than .5 m).

The first model makes the assumption of planar segmentation. According to this model, the *2D-planar curvature model*, the $\log_{10}$ tangential velocity in a two-dimensional plane is related to the $\log_{10}$ of the two-dimensional planar curvature k by $\log_{10}\sqrt{v_u^2 + v_v^2} = C + \beta \log_{10}(1/k)$.

In this equation the velocity components v_u and v_v refer to the velocity components in the local 2D plane of the ellipse and Cassini shape or to the 2D plane of the spiral or ellipse for the 3D cone and the elliptical spiral.

The second model, '*3D-planar curvature model*', tests the hypothesis that 3D tangential velocity is related to the two-dimensional curvature k in the osculating plane according to

$$\log_{10}\sqrt{v_x^2 + v_y^2 + v_z^2} = C + \beta \log_{10}(1/k)$$

Here, tangential velocity is the length of the 3D tangential velocity vector and curvature k is the reciprocal of the radius of a tangent circle.

The third model assumes that the 3D vector of tangential velocity is related to the '*total curvature*' $K = \sqrt{k^2 + \tau^2}$ according to the relation $\log_{10}\sqrt{v_x^2 + v_y^2 + v_z^2} = C + \beta \log_{10}(1/K)$.

This model is compatible with the hypothesis that movement planning and execution takes place in 3D space and that the dynamics of movements is independent of the orientation of the movement path in 3D space. This model reduces to the first model for curved paths in a two-dimensional plane (like the spiral movements).

2.8. Statistics

SPSS 11.0.1 (LEAD Technologies, Inc) was used to test the significance of the differences between conditions of shape, orientation, and the number of windings for the slope β of the linear regression and for the correlation coefficients. Univariate ANOVA and Tukey post hoc tests are used to test the significance for differences between the results for the three stimulus shapes (spiral *vs* cone *vs* elliptical spiral), for the three orientations (frontal *vs* transversal *vs* sagittal orientation) and for the three models (2D-planar curvature *vs* 3D-planar curvature *vs* total curvature model). *T*-tests are used for identifying significant differences for the two winding numbers (two *vs* five windings) and for small or large radii (begin and end of spirals and cones). The ANOVA-analysis is used for parameter comparison, while the Mann–Whitney test is used for comparison of the correlation coefficients. A repeated-measure ANOVA did not reveal any significant differences between subjects. Therefore, this has not been addressed in detail in Section 3.

3. Results

3.1. Qualitative description of the results

In general subjects could accurately move the finger along the specified paths. Fig. 2 shows the position of the finger tip for a typical subject while tracing a spiral in the frontal plane with two windings (upper row), a horizontally oriented cone with five windings (middle row) and a vertically oriented elliptical spiral with two windings (bottom row). Each panel shows a superposition of several back-and-forth movements while

subjects traced the shapes. For each shape, Fig. 2 shows a quasi-three-dimensional view (first column) and two-dimensional projections in the z–y plane (frontal view; second column) and y–x plane (horizontal plane viewed from above; third column). Fig. 2 shows that subjects are quite reproducible in tracing the 3D virtual reality shapes. Subjects trace the shapes quite well in the frontal plane, but slightly less accurately in depth (x-axis). Perception in depth appears to be less accurate than in the y and z-direction, in agreement with earlier reports in the literature: systematic and variable errors in perception and pointing are largest in the depth direction (Admiraal et al., 2003; Mrotek et al., 2006; Flanders et al., 2006). This trend was seen in all subjects who participated in this experiment. Fig. 2 shows that movements of subjects are consistent and reproducible for each of the displayed figure shapes.

Fig. 3 shows position (upper panel), velocity (second panel), tangential speed (third panel) and radius (inverse of total curvature) (bottom panel) for tracing movements along a cone with five windings (same data as shown for the cone in Fig. 2). The y-component of position (dashed line) in the upper panel shows back-and-forth movements at a more or less constant velocity, while the x (solid line) and z-components (dotted line) illustrate the rotation components for the cone with increasing and decreasing radius. The velocity traces show that x- (solid line) and z-(dotted line) components are 90° out-of-phase. When the stimulus is traced progressively from the centre outwards in the first 9 sec, tangential velocity increases (third panel). This corresponds to an increasing radius of curvature of the cone path (fourth panel). The third and fourth panel, showing tangential speed (m/sec) and radius of curvature (m), clearly illustrate the covariation of speed and radius of curvature. The large peaks in the trace of radius (lower panel) reflect artifacts due to the fact that subjects stop the movement at a relatively high velocity at the end of the cone and prepare for reversal. These peaks were not included in the quantitative analysis to relate velocity to the inverse of curvature (see Section 2).

The data for the cone with five windings shown in Fig. 3 are representative for all subjects and for other movement paths. The results for the full data set are described in the following paragraphs.

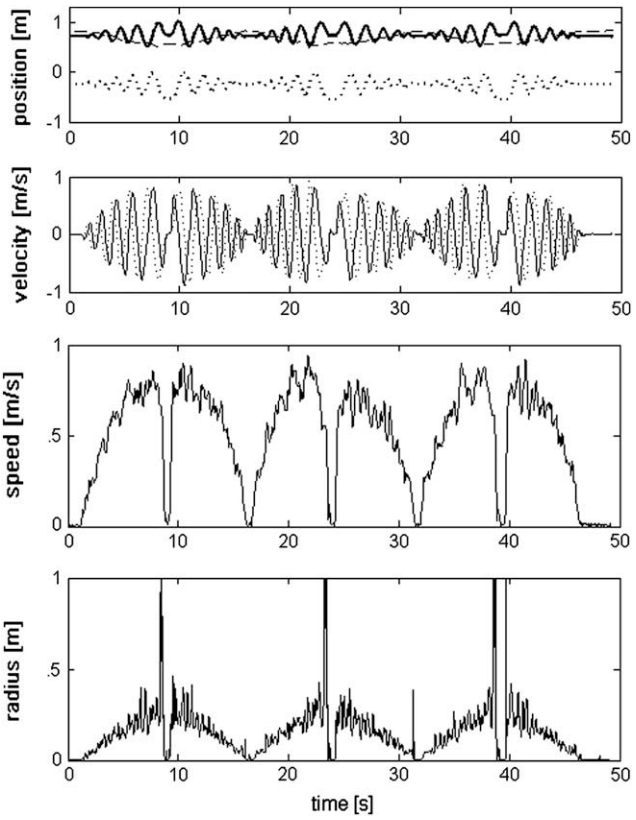

Fig. 3 – Position (top panel), velocity (second panel), tangential speed (third panel) and radius (bottom panel) for movements along a cone shape with five windings. The trajectory of the finger is shown for three movements in back-and-forth direction. The upper panel shows X (solid line), Y (dashed line) and Z (dotted line) components of position of the finger tip as a function of time. The second panel shows the X (solid line) and Z (dotted line) velocity components. The third panel shows the amplitude of tangential velocity. The fourth panel shows radius as a function of time. This signal shows some sharp peaks, which occur if the movement path is close to a straight line for a short amount of time, which happens if the subject stops the movement and prepares for reversal of the movement.

3.2. *Quantitative description of the results*

Table 1 shows the mean and standard deviation (SD) for the slope (β) of the linear regression and the square of the correlation coefficient (R^2) for the various stimulus shapes for the three models. Numbers between parentheses give the SD. The squared correlation coefficient gives the fraction of the variance, which is explained by the model. Mean values and SD for the three shapes are obtained by averaging over six values (stimuli in three orientations and two winding numbers). Similarly, the mean and SD for each orientation were obtained by averaging over three stimulus shapes, each with two windings numbers. The mean and SD for the winding numbers correspond to the average over nine values (three stimulus shapes in three orientations each). Overall means (bottom row in Table 1) are obtained from mean values of 10 subjects times 18 stimuli resulting in 180 values for β and R^2. The highest value R^2 is found for the *total curvature model*, indicating that this model explains most of the variance in the data.

The R^2 value appears to be consistently and significantly higher for the *total curvature model* than for the other two models for each of the conditions of stimulus shape, orientation and winding number. This was significant for each of these conditions (Mann–Whitney rank test; $p < .05$), indicating that this model explains most of the variance in the data. The R^2 values for the *total curvature model* were not significantly different for the three orientations of the stimuli, indicating that the same relations exist for movements in any direction in 3D. Interestingly, the *total curvature model* gives a significantly better fit for the planar 2D spiral stimuli than the *2D-planar curvature model*. Given the fact that the spiral stimuli are

Table 1 – Mean and SD of beta coefficients and the squared correlation coefficients for the three models (columns) for the spirals, cones and elliptical spirals in three orientations (frontal, transversal and sagittal) and with two winding numbers (two and five)

		2D-planar curvature model		3D-planar curvature model		Total curvature model	
		Beta (SD)	R^2 (SD)	Beta (SD)	R^2 (SD)	Beta (SD)	R^2 (SD)
Shape	Spiral	.34 (.09)	.68 (.12)	.34 (.09)	.68 (.12)	.36 (.08)	.72 (.11)*
	Cone	.37 (.07)	.69 (.10)	.36 (.08)	.61 (.12)	.39 (.06)	.73 (.08)*
	Elliptical spiral	.24 (.04)	.55 (.16)	.24 (.04)	.53 (.16)	.27 (.05)*	.67 (.14)*
Orientation	Frontal	.35 (.11)	.65 (.13)	.35 (.11)	.64 (.13)	.37 (.11)	.72 (.13)*
	Transversal	.29 (.07)	.65 (.13)	.28 (.07)	.58 (.14)	.31 (.07)	.69 (.13)*
	Sagittal	.31 (.07)	.63 (.16)	.31 (.07)	.60 (.16)	.34 (.07)	.72 (.12)*
Windings	2	.32 (.09)	.64 (.14)	.31 (.09)	.59 (.15)	.34 (.09)	.70 (.13)*
	5	.32 (.09)	.65 (.14)	.31 (.09)	.62 (.14)	.34 (.09)	.71 (.13)*
Mean		.32 (.09)	.64 (.14)	.31 (.09)	.61 (.15)	.34 (.09)	.71 (.13)*

Overall means and SD are presented at the bottom row. Asterisk * indicates a significant difference ($p < .01$) of that value for the ''total curvature model'' relative to the values of the other two models in that row.

planar, one would not have expected a significant difference between the results of the *total curvature model* and that of the *2D-planar curvature model*, since the *total curvature model* reduces to the *2D-planar curvature model* for planar stimuli. The most likely explanation relates to the fact that subjects, while tracing the planar 2D spiral, do not perfectly stay within the plane, but make small excursions in the third dimension. Since the *total curvature model* gives a better fit to the spiral data than the *2D-planar curvature model*, this implies that the small excursions in the third dimension are not simply noise, but represent an intrinsic part of the 3D nature of the motor programme.

For some conditions, such as for the cone stimulus and the transversal orientation, the R^2 values were significantly higher for the *2D-planar curvature* model, than for the *3D-planar curvature* model. This can be explained by the fact that the *3D-planar curvature* model searches for a linear correlation between the logarithm of the tangential velocity in 3D and the logarithm of 2D curvature, whereas the *2D-planar curvature* model seeks for a linear correlation between the logarithm of the tangential velocity in 2D and the logarithm of 2D curvature. Presumably, the third dimension of velocity in the regression for the *3D-planar curvature* model, which does not correspond to the two components that are used to calculate the planar curvature, acts as a noise term, which reduces the correlation coefficient.

The R^2 value near .71 for the *total curvature model* means that 29% of the variance is not explained by the *total curvature model*. The smallest value for R^2 was found for the elliptical spiral shapes. This small value is partly an artifact of the elliptical spiral shape. For this stimulus shape the planar curvature κ varies over a small range and torsion τ is constant. Consequently, also the total curvature varies over a small range of values. If tangential velocity is a function of curvature, a small range of curvatures implies a small range of tangential velocities. Because of the small range of curvatures and tangential velocities, the fit between tangential velocity and curvature is vulnerable to noise. This is compatible with the relatively high SD for R^2 values for the elliptical spiral shapes. If we take out the data for the elliptical spiral shapes, the overall mean values for R^2 increase to .69, .65 and .72 for the *2D-planar curvature*, *3-planar curvature* and *total curvature* model, respectively. The R^2 squared values were significantly larger for the *total curvature model* than for the other models, indicating that movements are intrinsically 3D and that 3D tangential velocity and total curvature should be included in the power law, rather than 2D values for tangential velocity and curvature.

Table 1 shows that the mean values for the regression slope β beta are close to the observed values of .33 in the literature. Any differences for overall mean values of the three models were not significant. Neither did the number of windings (smaller torsion values) affect the slope of the linear regression. However, β values were significantly higher for movements in the frontal plane than for movements in the transversal plane for all three models.

The results indicate that movement characteristics should be analyzed in 3D and argue against the notion of planar segmentation. This result is supported by the data shown in Fig. 4, which shows torsion for movements of the finger along a cone with five (A) and two (B) windings, respectively. Planar segmentation implies a concatenation of planar segments, which would give rise to discontinuous changes in torsion. Fig. 4 shows that this is not the case. Values for torsion are small at the base of the cone, where the radius of the circular movement is large, and torsion increases when the radius of the movement decreases (see explanation in Section 2). Rapid changes in torsion happen at the start and end of the movement along the cone, where the finger stops for the return movement. When finger velocity is near 0, small amounts of noise in position give rise to large artifacts in torsion. Apart from the large values at the start and end of the movements along the cone, torsion changes continuously, arguing against planar segmentation.

3.3. *Coordination of eye and finger movements*

Fig. 5 shows a quasi 3D view of finger path (grey lines) and gaze path (black line) while tracking a target moving along the

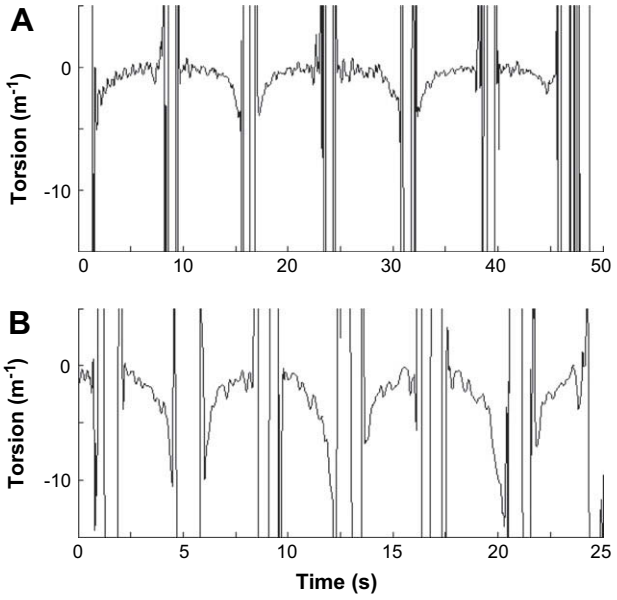

Fig. 4 – Torsion of the finger path when moving along a cone with five windings (A) and with two windings (B). Values for curvature varies are small at the base of the cone, where the radius of circular movement is large, and increases toward the top of the cone. When the movement returns (at the top and at the base of the cone), torsion is not defined, which explains the large and rapidly changing values.

Cassini shape (panel A) and for tracing the Cassini shape (panel B). Each panel shows data for three repetitions of tracking and tracing, respectively. Panel A shows that gaze and finger position superimpose almost perfectly during smooth pursuit tracking, except for short-lasting changes in depth during blinks and during saccades. The change in vergence during saccadic eye movements is well known in the literature (Chaturvedi and Van Gisbergen, 1998; Sylvestre et al., 2002). It is thought to be due to the different dynamics of centripetal and centrifugal saccades, which causes different saccadic trajectories for the two eyes (see e.g., Enright, 1984; Collewijn et al., 1988, 1997; Erkelens et al., 1989a, 1989b). During tracing, consistent smooth pursuit eye movements are not possible and gaze moves along the Cassini shape by a sequence of saccades. This becomes evident by the sequence of clusters of points, corresponding to the positions of fixation. Panel C shows gaze for a single cycle during tracing of the Cassini shape (second cycle of the three tracing cycles).

The X-, Y- and Z-components of the index finger (grey line) and of gaze position (black line) are shown in Fig. 6 for tracking (upper row) and tracing (third row) as a function of time. The upper row shows the data for the tracking condition, while the subject tracks a target moving along the Cassini shape. In the tracking condition, position of the eye and hand almost perfectly superimpose, especially for the Y (azimuth) and Z (elevation) component. Clearly the noise in gaze position is much larger in depth (X-direction) than for azimuth and elevation. The small negative peaks in depth (X) component of gaze position correspond to small saccades, which are visible as rapid shifts in the Y- and Z-components of gaze.

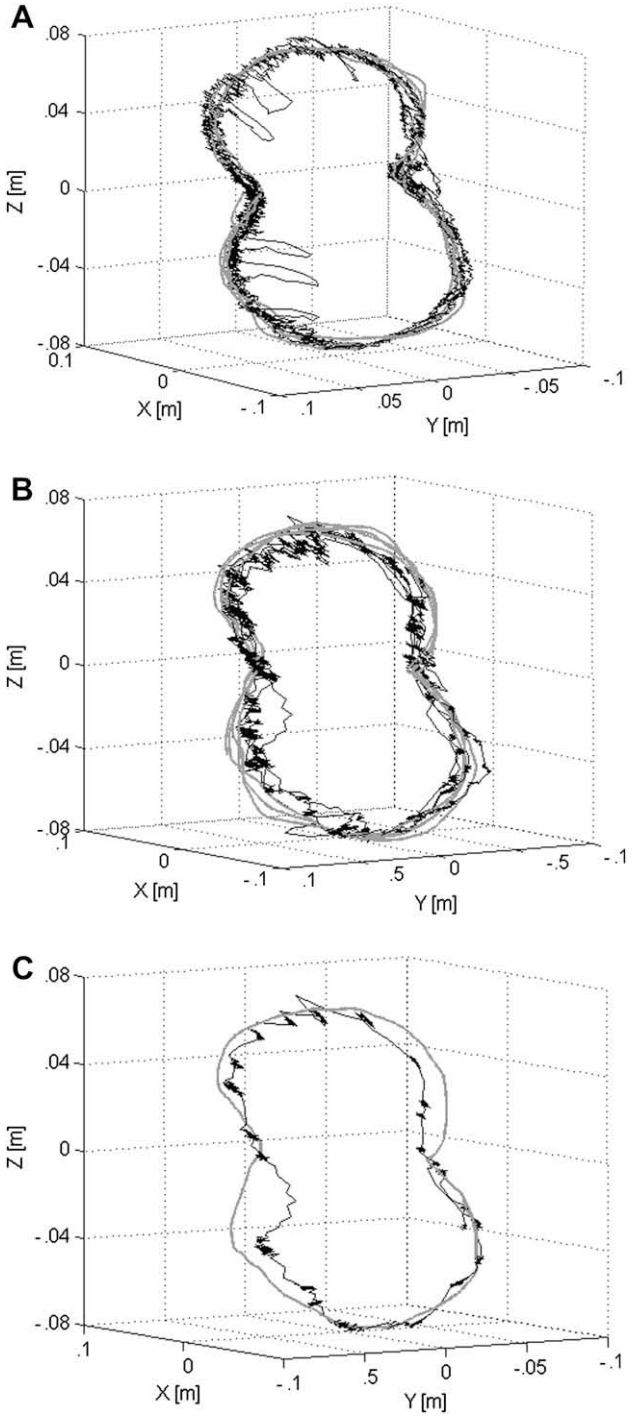

Fig. 5 – Position of the eyes (black line) and position of the hand (grey line) are shown while the subject was tracking (A) and tracing (B) the Cassini shape, rotated over 45° along the horizontal axis. Panel A and B show three repetitions each. Panel C shows a detailed view of eye position for the second trial of the three tracing cycles shown in B.

In the tracing condition (panels in third row) the coordination of gaze position and finger position is clearly different from that in the tracking condition. First of all, gaze follows the target by smooth pursuit in the tracking condition. This is evident in the smooth gaze trajectories for the X-, Y- and

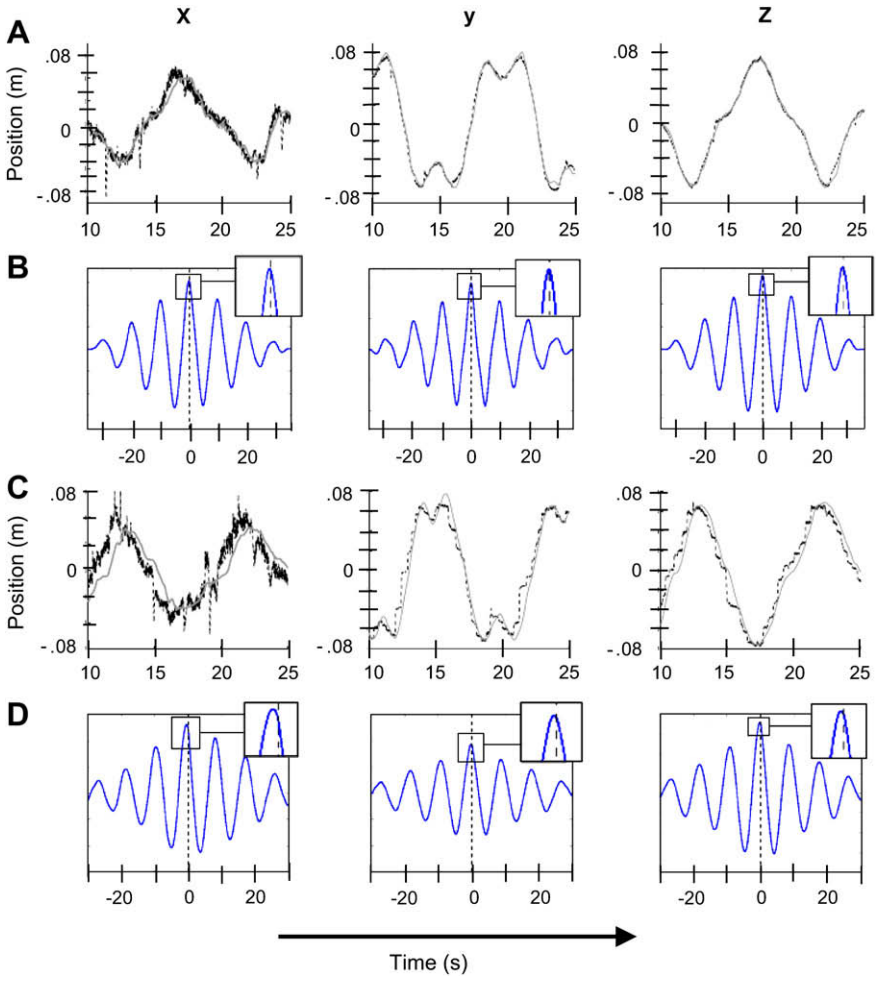

Fig. 6 – X-(left column), Y-(middle column) and Z-(right column) components of position of the finger tip (grey line) and of gaze position (black line) for tracking (upper row panels, A) and tracing (panels in third row, C) of the Cassini shape, rotated over 45° along the horizontal axis. These signals are from the second cycle in the sequence of three repetitions for each condition. The panels in the second (B) and fourth row (D) show the results of the cross-correlation between position of the finger tip and of gaze. A peak in the cross-correlation at negative time indicates that eye position leads the position of the finger tip. The insets for B and D show an enlarged view of the peak of the cross-correlation near $\tau = 0$ s.

Z-components of gaze. In the tracing condition, the depth (X-)component looks like some kind of smooth movement with a superposition of changes in depth related to saccadic gaze shifts (Y- and Z-components). The Y- and Z-components of gaze in the tracing condition clearly show a sequence of saccades. The second difference is that during tracing, the depth component of gaze clearly leads the finger (left panel in third row). The Y- and Z-components of gaze reveal many saccades (second and third panel in third row). The general observation is that the gaze jumps to a new position on the Cassini shape and stays there until the hand has reached this position. As soon as the hand has reached that position, gaze moves to another position on the Cassini shape. Very similar results were obtained for the 3D cone stimuli and the elliptic cylinder shapes.

The different relative timing of gaze position and finger position can be quantified by the cross-correlation function between gaze position and finger position. Before calculating the cross-correlation function, the short-lasting changes in vergence during saccades were eliminated from the X-component of the gaze signal and the removed data-samples were interpolated using cubic splines.

The cross-correlation function between two signals has a peak around the origin for signals that are similar but slightly shifted in time relative to one another. The implication is that in such a case, the location of this peak denotes that precise time shift. The cross-correlation functions shown in Fig. 6B usually have a peak near 0 for the tracking condition. The mean values averaged over all stimuli were −23 msec (SD = 38 msec) and −42 (SD = 28 msec) for the Y- and Z-components in the tracking condition, with negative values indicating that gaze position leads finger position (see Table 2). The mean value was not significantly different from 0 for the Y-component, but was significantly different from 0 for the Z-component ($p < .01$). Although gaze leads the finger position by a small amount in the tracking condition, this is hardly visible in the Y- and

Z-components of the position traces of finger and gaze in Fig. 6A. This is different for the X-(vergence) component. On average gaze has a significant ($p < .01$) lead on finger position for changes in depth (mean −266 msec; SD = 225 msec). This mean value is obtained by averaging the time lead for all stimuli. The time lead was not significantly different for different stimulus shapes (Cassini shape, cone and elliptic cylinder).

In the tracing condition, the lead of gaze relative to finger position is much larger. The mean values for the time lead of gaze relative to the finger are −220 msec (SD = 150 msec) and −230 msec (SD = 150 msec) for the Y and Z-direction, respectively. These values were significantly different from 0. They are also significantly larger than in the tracking condition. The lead of gaze is obvious from Fig. 6, which shows that a saccade moves gaze to a new position along the shape, where gaze remains fixed until the finger had reached that position, which then gives rise to a saccade to a new position along the shape. For the X-component, gaze leads finger position by 390 msec (SD = 230 msec). This lead time is significantly larger than the lead times for the X- and Y-components and also significantly larger than for the tracking condition.

The cross-correlation results show that eye position leads finger position. Moreover, a close look at Figs. 6B and 5B, C reveals that saccades bring gaze to various positions along the Cassini shape. Subjects always fixate at the positions of highest curvature, but fixate also on other positions along the Cassini shape. In fact, no clustering of fixation near positions of high curvature seems evident. This raised the question whether gaze position leads finger position by a constant time, or whether gaze position leads finger position by a constant spatial distance. If we assume that gaze leads finger position by a constant time with constant time intervals between saccades, saccades should have larger amplitudes near small curvatures, where the power law predicts high velocities of the finger. However, if we assume that gaze leads finger position by a constant distance, one might expect that all saccades have the same amplitude and that the interval of saccades is shorter at low curvatures, where finger velocity is high. Of course, these hypotheses reflect two rather extreme strategies and intermediate strategies are possible as well. To discriminate between these models, we have plotted the amplitude of saccades as a function of curvature of the Cassini shape. This revealed a high negative correlation (mean correlation −.8; SD = .2) with large saccades for small curvatures in the stimulus path (high finger velocities). We also explored the mean time interval between subsequent saccades. This revealed an almost constant time interval of about 625 msec (mean value 621 msec; SD = 147 msec). There was no significant correlation between the interval of saccades and curvature of the path. This implies that the most likely interpretation is that gaze leads the finger by a constant time by a regular pattern of saccades, such that gaze shifts are larger when the hand moves faster.

Analysis of the β-coefficients of the power law fit gave results in agreement with the results of the first experiment in this study. These results were also in agreement with the results reported by Flanders et al. (2006), who also reported on the power law for finger movements along a Cassini shape.

Table 2 – Mean values (SD between parentheses) of the peak in the cross-correlation function between eye position and hand position for azimuth, elevation and depth for the tracking condition and tracing condition

	Azimuth	Elevation	Depth
Tracking	−23 msec (38 msec)	−42 msec (28 msec)	−266 msec (175 msec)
Tracing	−220 msec (125 msec)	−230 msec (125 msec)	−390 msec (180 msec)

Negative value implies that the eye leads the hand. These values are obtained by averaging over all subjects and all stimulus shapes.

4. Discussion

In this study we have addressed two related problems. The first problem relates to the question whether movements in 3D are basically a concatenation of 2D-planar movement segments or whether all three orthogonal components of movements are an integral part of the movement. To answer this question we have investigated the two-thirds power law for three-dimensional movements in human subjects. This law describes a nonlinear relationship between tangential velocity and radius of curvature of the end-effector trajectory. Our study showed that the best fit is obtained by including three-dimensional tangential velocity and three-dimensional curvature (the so-called total or third curvature, rather than the planar curvature). This shows that the power law holds for three-dimensional trajectories and that all three orthogonal components of the movement form an integral part of the movement. 3D movement space forms an isotropic homogeneous space with regard to characteristics of the power law. This conclusion is supported by the observation that torsion of 3D movements changes continuously, rather than discontinuously as one would expect for a concatenation of planar movement segments. Therefore, we conclude that movements in 3D are truly three-dimensional.

The second problem addressed the coordination of eye and hand movements. The results reveal a tight coordination between gaze and finger movements. When tracking a moving target gaze leads finger position by a small amount (20–40 msec) for azimuth and elevation, and with a lead time of about 250 msec for movements in depth (vergence). For tracing (drawing) a 3D-shaped figure, gaze leads the finger, as is well known from the literature (Neggers and Bekkering, 1999; Ariff et al., 2002; Vaziri et al., 2006). The lead time is about 220 msec for azimuth and elevation, and about 390 msec for the depth (vergence) direction. The different lead times of gaze for vergence and direction argue against the simple idea that the power law reflects a general mechanism, which underlies the control of eye and arm movements.

In Section 4, we will first discuss the power-law fit and the relation between the power law and three different regression methods and its implications for motor control. After that, we will discuss the implications of the different lead times of gaze (in vergence and version direction) on eye-hand coordination.

4.1. *Power law fit*

Most studies in the past, testing the two-thirds power law, have studied planar (2D) movements, like ellipses, cloverleaves, and ''figures eight''. These studies have revealed that the power law gives a good fit between the logarithm of curvature of the movement path and the logarithm of tangential velocity in two-dimensional space. Our study confirms this finding by reproducing the results for the two-dimensional spiral movements. However, in daily life movements are performed in three-dimensional space. Our results show that the *total curvature model* gives a significantly better fit for 3D movements than models, which relate tangential velocity to two-dimensional curvature. Most of the variance in the power-law fit is explained by the *total curvature model*. Therefore, we conclude that 3D tangential velocity is correlated with 3D (total) curvature. Consequently, movement generation is intrinsically three-dimensional.

Considering the number of windings, no significant differences were found. Apparently, torsion of the shape has no effect on the power-law fit by the *total curvature model*. This adds further support to the *total curvature model*, which takes account of torsion. The *2D* and *3D-planar curvature models* do not take torsion into account.

Regarding the orientations of the shapes, significant differences exist for the beta coefficient and for the explained variance for different orientations. For the *total curvature model*, frontally oriented shapes have larger beta coefficients compared to transversally oriented shapes. This difference was significant and agrees with similar results obtained by Schaal and Sternad (2001). These authors reported differences for the beta coefficient for frontal and transversal orientations, which became larger for larger movement amplitudes. Sagittal shapes appeared to have intermediate beta coefficients in our study. To explain the different exponent in the power law for movements in the frontal and transversal plane Schaal and Sternad (2001) postulated that the power law is valid in joint space and that the difference for the beta coefficients for the frontal and transversal shapes might reflect the nonlinear transformation between joint coordinates and work-space coordinates. Due to the nonlinear transformation between joint coordinates and work-space coordinates, the beta coefficient will differ from the value 1/3 for larger movements. A seven-degree of freedom robot whose endpoint trajectories were generated based on the human joint angle data, modelled as simple harmonic oscillations, produced the same systematic violations. Schaal and Sternad, therefore, concluded that subjects employed smooth oscillatory patterns generation in joint space to realize the required movement patterns and that the precise exponent of the nonlinear relationship between tangential velocity and curvature in work space depends on the transformation between joint coordinates and work-space coordinates.

4.2. *Gaze-finger coordination*

The results in this study show that the relative timing of changes in gaze direction and changes of gaze in depth direction is different during tracking a moving target and during tracing a completely visible path. During tracking, changes of gaze in depth direction precede finger movements by about 265 msec, whereas changes in gaze direction lead the finger movements by about 20–40 msec. For the tracing condition, these numbers are about 400 msec for depth and about 200 msec for directional gaze changes. These data show that the control of gaze in depth has a different timing than the control of directional gaze changes. This is compatible with the idea, that the control of vergence and saccades is mediated by different neuronal structures with different dynamics.

Because of the conduction times of spikes along the nerve fibres from motor cortex to spinal cord and from the spinal cord to the muscles, and due to contributions of inertia of the arm, the onset of arm movements is always later than onset of eye movements if the central nervous system would generate the motor command for eye and arm movements simultaneously. Since it is well known that EMG activity begins as much as 100 msec prior to arm movements (Wadman et al., 1980; Karst and Hasan, 1991) and considering that the conduction time from motor cortex to arm muscles is at least 20 msec, a synchronous initiation of motor commands in the CNS would predict that eye movements lead arm movements by about 120 msec. The results from this study show that the eye leads the finger movement in the tracking condition by about 265 msec for depth, and by about 20–40 msec for changes in direction. This would imply that the motor command for vergence eye movements precedes the motor command for finger movements in the CNS, and that the generation of changes in gaze direction is generated after the motor command for the finger (see also Gribble et al., 2002). For the tracing condition, the lead times for gaze are larger than 200 msec for directional gaze changes and almost 400 msec for changes in vergence. This implies that the planning and execution of eye movements in the tracing condition precede the execution of the motor command for finger movements, which is in agreement with the hypothesis that eye movements assist in anticipation and planning of finger movements. However, we want to stress that anticipation only may be too simplistic a view. The time lead of gaze movements in the *x*-dimension does not seem to configure a case of anticipation, as true anticipation would imply an almost fixed lead time in all three dimensions. Therefore, our results to point to a more complex process than simple anticipation by a constant lead time.

Differences in lead times of the vergence component of gaze relative to stimulus motion have been reported before. Erkelens et al. (1989a) found that vergence has a delay relative to target motion when tracking a target motion controlled by the experimenter. However, when the subject controls target motion in depth, e.g., when using the hand to move the target, vergence leads target motion by about 100 msec. This implies that when the subject can somehow predict upcoming target positions, like in the tracing condition, vergence may have a larger lead time than when target motion is less predictable (like in the tracking condition).

In a previous study, de'Sperati and Viviani (1997) asked subjects to track targets, moving along an ellipse, with smooth pursuit eye movements. These authors varied the kinematics

of target motion and found that smooth pursuit was most accurate (i.e., smallest number of saccades) when target movements were compatible with the two-thirds power law. This result, combined with the observation that the relation between curvature and velocity of the smooth component of tracking did not depart much from that prescribed by the power law, led these authors to the conclusion that the two-thirds power law reflects a general neural mechanism which is common to distinct control modules, e.g., for the arm and eye. Our results reveal clear differences between gaze and finger movements in the tracking and tracing conditions with regard to smooth pursuit versus saccadic eye movements and regarding the timing of gaze relative to finger position. These differences argue against the generality of the power law for arm and hand movement control. However, this conclusion may be too simplistic, since it does not take into account some of the complexity of the motor system and assumptions underlying the power law. The vergence and version control system are known to be distinct (and in fact located in different brain nuclei). This fact does not preclude or contradict the fact that each of these subsystems may operate in a manner that is consistent with the power law. Indeed, several studies have shown that smooth pursuit version (i.e., direction) control exhibits clear power law behaviour. The saccadic system has different dynamics which are not assumed to show the same power law behaviour. This partition in oculomotor function mirrors, perhaps, the original observation of the power law in smooth hand movements, as opposed to point-to-point movements.

A frequency analysis by de'Sperati and Viviani (1997) revealed the presence of anticipation in the oculomotor system. The anticipation fits very well with the fact that gaze position leads finger position in the tracing condition. A saccadic eye movement brings gaze to a new position on the path of the stimulus and gaze remains there until the finger reaches that position. At that time a new saccade brings gaze to a next position. This anticipation may be important to plan a smooth trajectory for the finger. Previous studies have shown that the two-thirds power law follows from minimum-jerk optimal control. The planning of minimum-jerk movements requires anticipation and the lead of gaze position may be important for good anticipation.

The observation that gaze leads finger position is in agreement with earlier results by Ariff et al. (2002). These authors measured eye position (monocular eye position and therefore only directional components of gaze were measured) when subjects were instructed to track an unseen reaching movement. They found that saccade occurrence at any time t consistently provided an unbiased estimate of hand position at time $t + 196$ msec. This agrees perfectly with the time lead of about 200 msec for the Y- and Z-components of gaze while tracing a 3D shape with the finger in our study (see also Fig. 6). This results is in agreement with the idea that the brain computes an estimate of future hand position during reaching and drawing with the hand based on an internal model that relies on real-time proprioceptive feedback (Ariff et al., 2002).

These ideas are also in agreement with earlier suggestions by Johansson et al. (2001) who reported that gaze supports hand movement planning by fixating at future critical landmarks during the movement, suggesting that gaze supports predictive motor control in reaching, grasping and object manipulation.

There has been a long debate as to whether target position is represented in the brain in a body-centred frame of reference, in extrinsic work-space coordinates, or in an eye-centred frame of reference. Recent behavioural studies (Henriques et al., 1998, 2003; van Pelt and Medendorp, 2007) have shown that updating of target position during active whole-body rotations or head movements takes place in a gaze-centred frame of reference. Moreover, neuroimaging studies and electrophysiological recordings in cortex have shown that target position is represented in parietal cortex and in medial inter-parietal in eye-centred coordinates (Buneo et al., 2002; Medendorp et al., 2005; Pesaran et al., 2006). This implies that hand position, as derived from proprioceptive information, is transformed ''backwards'' into an eye-coordinate frame of reference to map the effector and target position in the same frame of reference (Medendorp et al., 2005). The fact that gaze leads finger position, possibly to help the brain in computing and planning of future hand positions, may provide one more reason why target position is represented in eye-centred coordinates, rather than in body-centred coordinates or in a world frame of reference. Recently, Admiraal et al. (2003, 2004) investigated pointing movements toward remembered targets after an intervening self-generated body movement. In their study subjects were asked to fixate at a visual target. When the target disappeared, subjects had to make an active whole-body displacement followed by a pointing movement to the remembered target position. Obviously, these pointing movements were not perfectly accurate and neither was the fixation position after the body displacement. The covariation between gaze and pointing position reflects that pointing accuracy depends on fixation. Apparently, gaze acts like an anchor for accurate movements of the hand.

The gaze data indicate that during tracing (drawing) the eyes lead finger position. However, the lead time is different for directional gaze components and for vergence. This raises the question why the lead time of gaze is much larger for depth (X-direction) than for azimuth and elevation. A possible explanation might be related to the fact that pursuit velocities in vergence direction are typically much smaller than pursuit velocities in azimuth and elevation. Erkelens et al. (1989a, 1989b) reported that vergence velocities are much faster than previously thought (maximum pursuit velocities between 50 and 100°/sec). However, since vergence velocities never reach saccadic velocities (typically between 200 and 800°/sec) vergence movements are not as fast as changes in gaze direction. Therefore, if gaze should lead finger position by a particular distance for appropriate anticipation and planning of finger movements, then a larger lead time may be necessary for vergence than for azimuth and elevation because *lead distance* equals *lead time* multiplied by gaze velocity.

Our results clearly indicate that movement trajectories reflect a truly 3D nature: the best fit for movement parameters requires that all three movement dimensions are included in the model. Our results also showed differences between gaze and finger movements in the tracking and tracing condition, with a larger lead time for gaze in the depth direction.

REFERENCES

Admiraal MA, Keijsers NLW, and Gielen CCAM. Interaction between gaze and pointing toward remembered visual targets. *Journal of Neurophysiology*, 90: 2136–2148, 2003.

Admiraal MA, Keijsers NLW, and Gielen CCAM. Gaze affects pointing toward remembered visual targets after a self-initiated step. *Journal of Neurophysiology*, 92: 2380–2393, 2004.

Ariff GA, Donchin O, Nanayakkara T, and Shadmehr R. A real-time state predictor in motor control: study of saccadic eye movements during unseen reaching movements. *The Journal of Neuroscience*, 22: 7721–7729, 2002.

Buneo CA, Jarvis MR, Batistia AP, and Andersen RA. Direct visuomotor transformations for reaching. *Nature*, 416: 632–636, 2002.

Chaturvedi V and Van Gisbergen JAM. Shared target selection for combined version-vergence eye movements. *Journal of Neurophysiology*, 80: 849–862, 1998.

Collewijn H, Erkelens CJ, and Steinman RM. Binocular co-ordination of human horizontal saccadic eye movements. *Journal of Physiology (London)*, 404: 157–182, 1988.

Collewijn H, Erkelens CJ, and Steinman RM. Trajectories of the human binocular fixation point during conjugate and non-conjugate gaze shifts. *Vision Research*, 37: 1049–1069, 1997.

Enright JT. Changes in vergence mediated by saccades. *Journal of Physiology (London)*, 350: 9–31, 1984.

Erkelens CJ, Steinman RM, and Collewijn H. Ocular vergence under natural conditions. I. Continuous changes of target distance along the meridian plane. *Proceedings of the Royal Society of London B Biological Sciences*, 236: 417–440, 1989a.

Erkelens CJ, van der Steen J, Steinman RM, and Collewijn H. Ocular vergence under natural conditions. II. Gaze shifts between real targets differing in distance and direction. *Proceedings of the Royal Society of London – B: Biological Sciences*, 236: 441–465, 1989b.

Flanders M, Mrotek LA, and Gielen CCAM. Planning and drawing complex shapes. *Experimental Brain Research*, 171: 116–128, 2006.

Flash T and Hogan N. The coordination of arm movements: an experimentally confirmed mathematical model. *The Journal of Neuroscience*, 5: 1688–1703, 1985.

Flash T and Handzel AA. Affine differential geometry analysis of human arm movements. *Biological Cybernetics*, 96: 577–601, 2007.

Gribble PL, Everling S, Ford K, and Mattar A. Hand-eye coordination for rapid pointing movements. *Experimental Brain Research*, 145: 372–382, 2002.

Harris CM and Wolpert DM. Signal-dependent noise determines motor planning. *Nature*, 394: 1727–1739, 1998.

Henriques DYP, Klier EM, Smith MA, Lowy D, and Crawford JD. Gaze-centered remapping of remembered visual space in an open-loop pointing task. *The Journal of Neuroscience*, 18: 1583–1594, 1998.

Henriques DYP, Medendorp WP, Gielen CCAM, and Crawford JD. Geometric computations underlying eye-hand coordination: orientations of the two eyes and the head. *Experimental Brain Research*, 152: 70–79, 2003.

Johansson RS, Westling G, Bäckström A, and Flanagan JR. Eye-Hand coordination in object manipulation. *The Journal of Neuroscience*, 21: 6917–6932, 2001.

Karst GM and Hasan Z. Timing and magnitude of electromyographic activity for two-joint arm movements in different directions. *Journal of Neurophysiology*, 66: 1594–1604, 1991.

Lacquaniti FC, Terzuolo CA, and Viviani P. The law relating the kinematic and figural aspects of drawing movements. *Acta Psychologica*, 54: 115–130, 1983.

Leigh RJ and Zee DS. *The Neurology of Eye Movements*. Philadelphia: F.A. Davis, 1983.

Mays LE. Neural control of vergence eye movements: convergence and divergence neurons in midbrain. *Journal of Neurophysiology*, 51: 1091–1108, 1984.

Medendorp WP, Goltz HC, Crawford JD, and Vilis T. Integration of target and effector information in human posterior parietal cortex for the planning of action. *Journal of Neurophysiology*, 93: 954–962, 2005.

Mrotek LA, Gielen CCAM, and Flanders M. Manual tracking in three dimensions. *Experimental Brain Research*, 171: 99–115, 2006.

Morasso P. Three dimensional arm trajectories. *Biological Cybernetics*, 48: 187–194, 1983.

Neggers SF and Bekkering H. Integration of visual and somatosensory target information in goal-directed eye and arm movements. *Experimental Brain Research*, 125: 97–107, 1999.

Pelizzer G, Massey JT, Lurito JT, and Georgopoulos AP. Three-dimensional drawings in isometric conditions: planar segmentation of force trajectory. *Experimental Brain Research*, 92: 326–337, 1992.

van Pelt S and Medendorp WP. Gaze-centered updating of remembered visual space during active whole-body translations. *Journal of Neurophysiology*, 97: 1209–1220, 2007.

Pesaran B, Nelson MJ, and Andersen A. Dorsal premotor neurons encode the relative position of the hand, eye, and goal during reach planning. *Neuron*, 51: 125–134, 2006.

Richardson MJA and Flash T. Comparing smooth arm movements with the two-thirds power law and the related segmented-control hypothesis. *The Journal of Neuroscience*, 22: 8201–8211, 2002.

Sternad D and Schaal S. Segmentation of endpoint trajectories does not imply segmented control. *Experimental Brain Research*, 124: 118–136, 1999.

Schaal S and Sternad D. Origins and violations of the 2/3 power law in rhythmic three-dimensional arm movements. *Experimental Brain Research*, 136: 60–72, 2001.

Soechting JF and Terzuolo CA. Organization of arm movements. Motion is segmented. *Neuroscience*, 23: 39–51, 1987a.

Soechting JF and Terzuolo CA. Organization of arm movements in three-dimensional space. Wrist motion is piecewise planar. *Neuroscience*, 23: 53–61, 1987b.

Soechting JF, Bueno CA, Hermann U, and Flanders M. Moving effortlessly in three dimensions: does Donders' law apply to arm movement. *The Journal of Neuroscience*, 15: 6271–6280, 1995.

de'Sperati C and Viviani P. The relationship between curvature and velocity in two-dimensional smooth pursuit eye movements. *The Journal of Neuroscience*, 17: 3932–3945, 1997.

Stoker JJ. *Differential Geometry*. New York: John Wiley & Sons, 1989.

Sylvestre PA, Galiana HL, and Cullen KE. Conjugate and vergence oscillations during saccades and gaze shifts: implications for integrated control of binocular movement. *Journal of Neurophysiology*, 87: 257–272, 2002.

Todorov E and Jordan MI. Smoothness maximization along a predefined path accurately predicts the speed profiles of complex arm movements. *Journal of Neurophysiology*, 80: 696–714, 1998.

Todorov E and Jordan MI. Optimal feedback control as a theory of motor coordination. *Nature Neuroscience*, 5: 1226–1235, 2002.

Vaziri S, Diedrichsen J, and Shadmehr R. Why does the brain predict sensory consequences of oculomotor commands?

Optimal integration of the predicted and the actual sensory feedback. *The Journal of Neuroscience*, 26: 4188–4197, 2006.

Viviani P and Terzuolo CA. Trajectory determines movement dynamics. *Neuroscience*, 7: 431–437, 1982.

Viviani P and Flash T. Minimum-jerk, two-thirds power law, and isochrony: converging approaches to movement planning. *Journal of Experimental Psychology: Human Perception and Performance*, 21: 32–53, 1995.

Wadman WJ, Denier van der Gon JJ, and Derksen RJ. Muscle activation patterns for fast goal-directed arm movements. *Journal of Human Movement Science*, 6: 19–37, 1980.

Wann JI, Nimmo-Smith, and Wing AM. Relation between velocity and curvature in movement: equivalence and divergence between a power law and a minimum-jerk model. *Journal of Experimental Psychology: Human Perception and Performance*, 14: 622–637, 1988.

Yarbus AL. *Eye Movements and Vision*. New York: Plenum, 1967.